NUCL SCI TECH (2017) 28:59
DOI 10.1007/s41365-017-0212-0

Influence of N_2 flow rate on structure and properties of TiBCN films prepared by multi-cathodic arc ion plating and studied with ion beam scattering spectroscopy

Bin Han[1] · **Ze-Song Wang**[1] · **D. Neena**[1] · **Bao-Zhu Lin**[1] · **Bing Yang**[2] ·
Chuan-Sheng Liu[1] · **De-Jun Fu**[1]

Received: 5 July 2016 / Revised: 13 October 2016 / Accepted: 2 November 2016 / Published online: 28 March 2017

Abstract TiBCN films were deposited on Si(100) and cemented carbide substrates by using multi-cathodic arc ion plating in C_2H_2 and N_2 atmosphere. Their structure and mechanical properties were studied systematically under different N_2 flow rates. The results showed that the TiBCN films were adhered well to the substrates. Rutherford backscattering spectroscopy was employed to determine the relative concentration of Ti, B, C and N in the films. The chemical bonding states of the films were explored by X-ray photoelectron spectroscopy, revealing the presence of bonds of TiN, Ti(C,N), BN, pure B, sp^2 C–C and sp^3 C–C, which changed with the N_2 flow rate. TiBCN films contain nanocrystals of TiN/TiCN and TiB_2/Ti(B,C) embedded in an amorphous matrix consisting of amorphous BN and carbon at N_2 flow rate of up to 250 sccm.

Keywords TiBCN · Nanocomposite · N_2 flow rate · Rutherford backscattering spectroscopy (RBS) · X-ray photoelectron spectroscopy

1 Introduction

Nitride-based protective films have been extensively studied due to their excellent properties such as high hardness and resistance against wear, erosion and corrosion. TiBCN is a promising nanocomposite film with good tribological properties, super high hardness and high resistance to oxidation and corrosion [1–5]. It is synthesized by chemical vapor deposition (CVD) [1, 2], cathodic arc plasma evaporation [3], thermal plasma CVD [4] and magnetron sputtering [5]. Depending on deposition conditions, the films of different microstructures, phase contents, morphologies and grain sizes can be produced. Multi-phase coatings of TiBCN consist of TiN, TiC, TiB_2, TiB and amorphous BN, C and CN_x, etc. By taking advantage of the high hardness phase of TiB_2 and TiC, and the low friction coefficient phase BN and CN_x, it is possible to fabricate TiBCN coatings with excellent mechanical properties by adjusting the atomic concentration of Ti, B, C and N.

Researchers have prepared TiBCN films on Si(100) substrate by reactive cathodic arc evaporation using the graphite/boron-containing composite target and Ti target in N_2 and C_2H_2 atmosphere. The cathode current of the target influenced composition and structure of the TiBCN films [3]. Shimada et al. [4] studied the composite TiBCN films deposited on WC–Co tools at 800 °C by varying the N_2 flow rate from 0 to 1000 mL/min and found that the N content in TiCN increased with the N_2 flow rate, but TiB_2 content decreased. Lin et al. [5] synthesized TiBCN nanocomposite films by sputtering compound target containing 80 mol.% TiB_2 and 20 mol.% TiC in Ar/N_2 plasma using a pulsed closed-field unbalanced magnetron sputtering system. They found that when the N content was low (3 at.%), the coating was characterized as a mixture of

---

This work was supported by the National Natural Science Foundation of China (Nos. 11375135 and 11275141), International Cooperation Program of the Ministry of Science and Technology of China (No. 2015DFR00720) and Fundamental Research Funds for the Central Universities.

✉ De-Jun Fu
djfu@whu.edu.cn

[1] Key Laboratory of Artificial Micro- and Nano-Materials of Ministry of Education and School of Physics and Technology, Wuhan University, Wuhan 430072, China

[2] School of Power and Mechanical Engineering, Wuhan University, Wuhan 430072, China

nanocolumnar grains of Ti(B,C) and small volume fractions of amorphous free carbon, BN and CN_x, while increasing the N content to 10–13 at.%, the N atoms would replace the B sites in Ti(B,C) leading to reduced Ti(B,C) phase and the formation of Ti(C,N), and an increase in the volume fraction of amorphous BN. When N content reached 36 at.%, the hard Ti(B,C) phase diminished completely, accompanied by the formation of a large volume fraction of amorphous BN.

Film compositions can be examined by several methods. X-ray photoelectron spectroscopy (XPS) is an efficient tool for determining the type of bonding states involving each element [6]. When the environment of the central atom becomes more electropositive, the peaks shift to lower energy, while it shifts to higher energy if the atom is bound to more electronegative neighbors [6]. XPS provides a relative amount of different phases, such as the carbon-containing phase as a function of the total carbon content [7]. It also provides depth profiles of elements by layer-etching (which takes much time and energy), but it is unable to provide accurate concentration of light elements, whereas they can be detected with Rutherford scattering spectroscopy (RBS), including non-elastic RBS, by using especially MeV protons to do nondestructive depth profiling with better sensitivity, smaller straggling and greater penetrability for light element detection.

In this work, TiBCN films were deposited by multi-cathodic arc ion plating at different flow rates of N_2. The samples were measured by X-ray diffraction (XRD), scanning electron microscopy (SEM), atomic field microscopy (AFM), high-resolution transmission electron microscopy (HRTEM), RBS and XPS, to observe the influence of N_2 flow rate.

2 Experimental section

All the samples were prepared by cathode ion plasma deposition, which are described in a previous report [8]. The Si(100) and cemented carbide substrates were ultrasonically cleaned by acetone, alcohol and de-ionized water. The sputtering targets were TiB_2 and metal Ti, with a target–sample distance of 100 mm.

The chamber was pumped to 1×10^{-3} Pa and the deposition substrate was kept at 300 °C. The samples were prepared as follows. First, the substrates were cleaned for 30 min by Ar^+ sputtering at a bias voltage of -800 V before Ti-ion etching to smooth the substrate surface. Then, Ti interlayer was deposited to improve adhesion and reduce stress at the coating–substrate interface. Finally, TiBCN films were deposited on the Ti interlayer. The deposition parameters are listed in Table 1. To ascertain the film homogeneity, all the substrates were rotated at a speed of 4 rpm. We note that a low flux of Ar gas could be fed into the chamber to enhance the efficiency of glow discharge during the process of Ti-ion etching. Particularly, C_2H_2 gas was set at a stable flow rate of 150 sccm at N_2 flow rates of 40–350 sccm during deposition using the TiB_2 target, while the Ti cathode was turned off. Ar gas was fed into maintain work pressure at 0.59 Pa for depositing TiBCN films. The samples were allowed to cool down to room temperature.

The samples were measured by X-ray diffraction (XRD, D8 ADVANCE) with Cu Kα ray ($\lambda = 0.1541$ nm). XPS (XSAM800 KRATOS) using Al Kα ray (1253.6 eV) was employed to investigate the samples' binding energy and elemental composition. The microstructure was examined by cross-view high-resolution transmission electron microscopy (HRTEM, JEOL JEM 2010). Field emission scanning electron microscopy (SEM, S4800) was used to measure the cross-sectional micrograph. The surface topography was probed on an atomic force microscope (AFM, Shimadzu SPM-9500J3) operated in the tapping mode with a probing area of 2 μm × 2 μm. The samples were measured by RBS using 1.62 MeV proton beams, with a detection angle of 165° using a planar silicon detector with a resolution of 14 keV at FWHM.

3 Results and discussion

XRD patterns of the TiBCN films grown on Si(100) substrate are shown in Fig. 1. The main peak at 40.17° is attributed to hexagonal Ti(101) (JCPDS No. 5-0682) [9] from the interlayer. The peaks at 35.1° and 38.36° are from interlayer Ti(100) and (002) or from $TiN_{0.3}$(100) and (002)

Table 1 Parameters of the experiment

Deposition step	Target current (A)	Bias voltage (V)	Temperature (°C)	Deposition time (min)	Ambient	Pressure (Pa)
Ar-ion etching	0	−800	300	30	Ar	2.0
Ti-ion etching	70	−800	300	10	Vacuum	2×10^{-2}
Ti interlayer	70	−200	300	10	Vacuum	2×10^{-2}
TiBCN	60	−200	300–350	30	$C_2H_2 + N_2 + Ar$	0.59

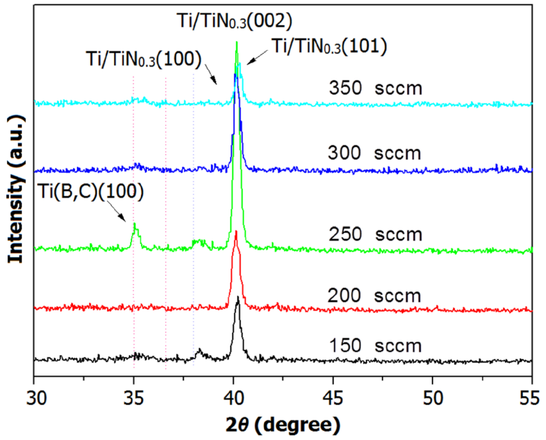

Fig. 1 XRD patterns of TiBCN coatings deposited on Si(100) substrate at different N_2 flow rates

in the TiBCN films. The two groups of peaks, which are very close (0.1° apart) to each other, are attributed to Ti and $TiN_{0.3}$, respectively. The attribution to TiN is based on chemical bonding of N–Ti (397.1 eV) and TiN (455.8 eV). The grain size of Ti/TiN crystals is 24.5–32.7 nm, calculated by Scherrer formula [10] using the peak (40.17°).

Intensity of the main peak increased with the N_2 flow rate up to 250 sccm, where it began to decrease. Above N_2 flow rates of 250 sccm, the grain size was smaller. This can be attributed to the corporation of N_2 into the growing film, which leads to a lower surface mobility [11]. The peak at around 35° can also be ascribed to TiB_2/Ti(B,C)(100) [7] and supported by Ti(B,C) (188.4 eV) from the following XPS B 1*s* spectra.

Figure 2 shows RBS spectra for the films deposited at N_2 flow rate of 40–350 sccm, with the simulated spectra (solid line) by SIMNAR. The RBS results of Ti, B, C and N concentrations in the samples are given in Table 2. The Ti concentration of TiBCN films, which was separated by subtracting Ti interlayer, almost keeps at 11% with varying N_2 flow rates. The B and C contents decreased with increasing N_2 flow rate from 18.9 to 9.4% and from 65.6 to 48.9%, respectively, while the N content increased with the N_2 flow rate from 3.9 to 29.3%. The atomic stoichiometry and depth profile of the films were obtained by fitting of the RBS data using SIMNRA. In Fig. 2a, a small peak at the left side is assigned to B from TiB_2 layer, and the ratio B to Ti is about 2:1. A broad nearby peak (left) of low intensity is attributed to Ti_xB_y with the ratio of Ti to B (x:y) from 9:1 to 8:2, which alludes that the boron atoms diffuse from TiB_2 layer into Ti interlayer, forming a gradient layer. The results are in accordance with the cross-sectional SEM images (Fig. 3), which reveal the three layers of TiBCN, TiB_2–Ti_xB_y, and Ti interlayer. Actually, high RBS cross section is only available between 1.62 MeV proton and Ti atom, while the other target atoms have just high non-Rutherford cross sections, with low resolution of mass difference for B, C and N with respect to incident proton, resulting in serious overlapping signals of these light elements. However, identifiable and prolific light elements in the sample can induce drastic non-Rutherford scattering

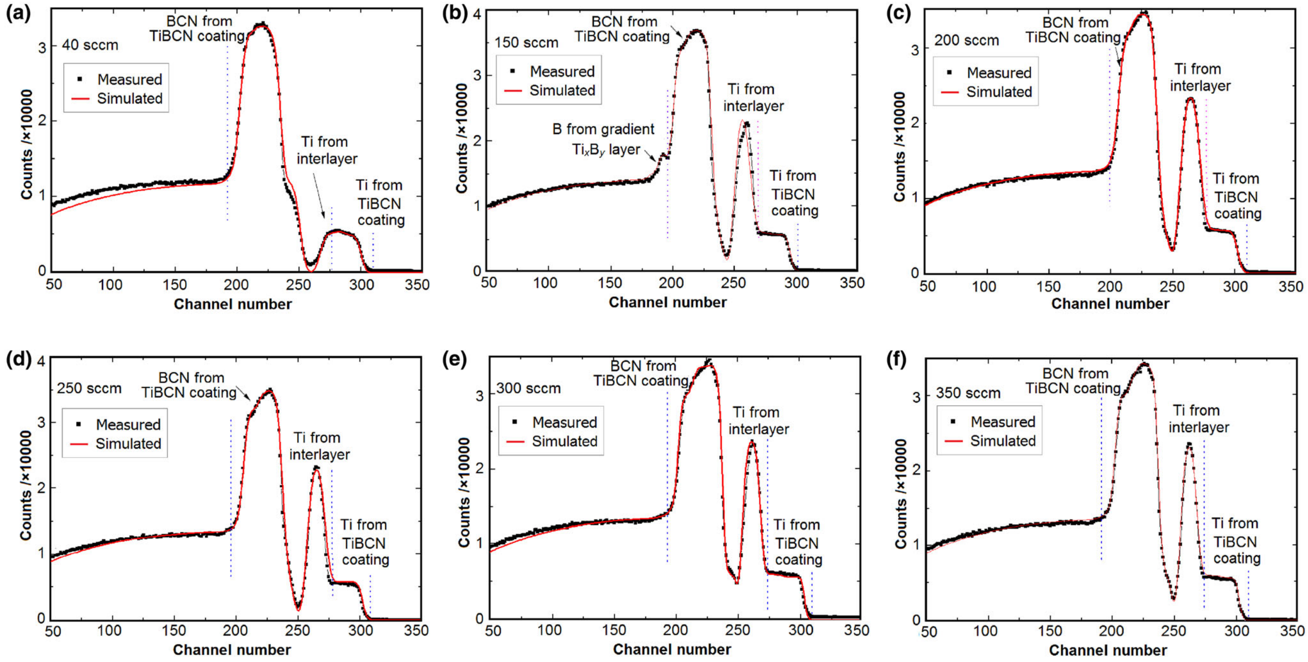

Fig. 2 RBS spectra of TiBCN films deposited at N_2 flow rates of 40–350 sccm

Table 2 Elemental concentration of Ti, B, C and N in TiBCN coatings prepared at N_2 flow rates of 40–350 sccm got from the RBS spectra

Sample no.	TiBCN-40	TiBCN-150	TiBCN-200	TiBCN-250	TiBCN-300	TiBCN-350
N_2 gas (sccm)	40	150	200	250	300	350
Ti (at.%)	11.54	10.80	11.44	11.86	11.74	11.80
B (at.%)	18.93	12.51	10.55	10.70	9.96	9.40
C (at.%)	65.63	56.34	52.80	54.56	48.95	50.40
N (at.%)	3.91	20.30	25.20	22.86	29.33	28.40
Average surface roughness, Ra(nm)		152.13	152.50	145.13	137.29	131.06
Sample thickness (μm)		2.20	2.04	1.91	2.10	1.86
Average grain size (nm)		27.50	24.50	30.10	28.90	32.70

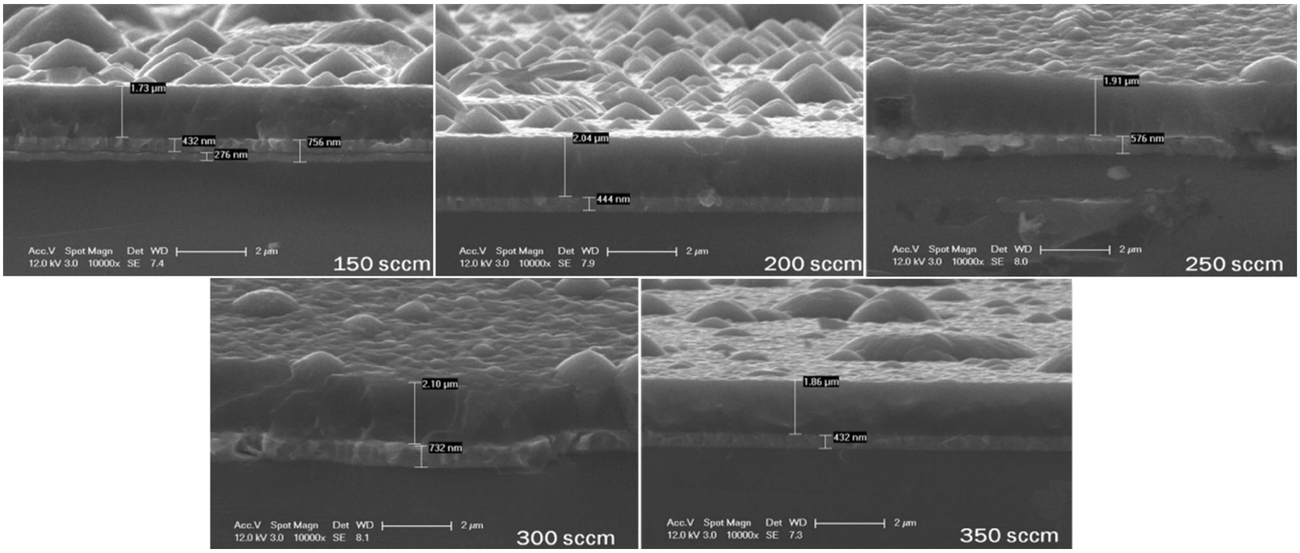

Fig. 3 Cross-sectional SEM of TiBCN films on Si(100) substrate deposited at N_2 flow rates of 150–350 sccm

cross sections by colliding with incident proton at ~MeV, which combined with SIMNRA fitting give their relative concentrations.

Figure 3 shows the cross-sectional SEM image of the TiBCN films. Although the deposition pressure was kept at 0.59 Pa in deposition of all the films, the micro-particle density on the surface is different. The flux of material emitted by either explosion or evaporation is composed of ions, neutral atoms, electrons and micro-droplets of the material. In arc ion plating, metal ions and micro-droplets are the main species responsible for the mass loss of the cathode, and unavoidably the particles would be deposited on the substrates [12]. The number of holes and micro-particles reduces with increasing nitrogen pressure up to 300 sccm, which could be attributed to the poison effect of TiB_2 targets surface. During arc evaporation, if successive reactive gas is present in the deposition chamber, then the cathode material can be poisoned by reactive gas resulting in formation TiN, which has a high melting point, covering the target surface. The surface became rougher and exhibited worse morphology with increasing nitrogen pressure up to 350 sccm. This could be attributed to the excessively reactive nitrogen gas weakening the ion bombardment [13]. Cross-sectional SEM of TiBCN-150 demonstrates that there are three layers: Ti interlayer, TiB_2–Ti_xB_y and TiBCN, which are confirmed by the RBS spectra and their fitting.

AFM images of the films are illustrated in Fig. 4. The root-mean-square (RMS) roughness decreases from 152.1 to 131.1 nm with increasing the N_2 flow rate, as summarized in Table 2. Instead of drastic jumps, there are some decreases in RMS roughness associated with larger N_2 fluxes, in agreement with nanocrystal size in the TiBCN films of XRD results.

The selective area diffraction (SAD) patterns of Ti interlayer and TiBCN films are shown in Fig. 5. The SAD pattern of Ti interlayer in Fig. 5a was indexed in terms of

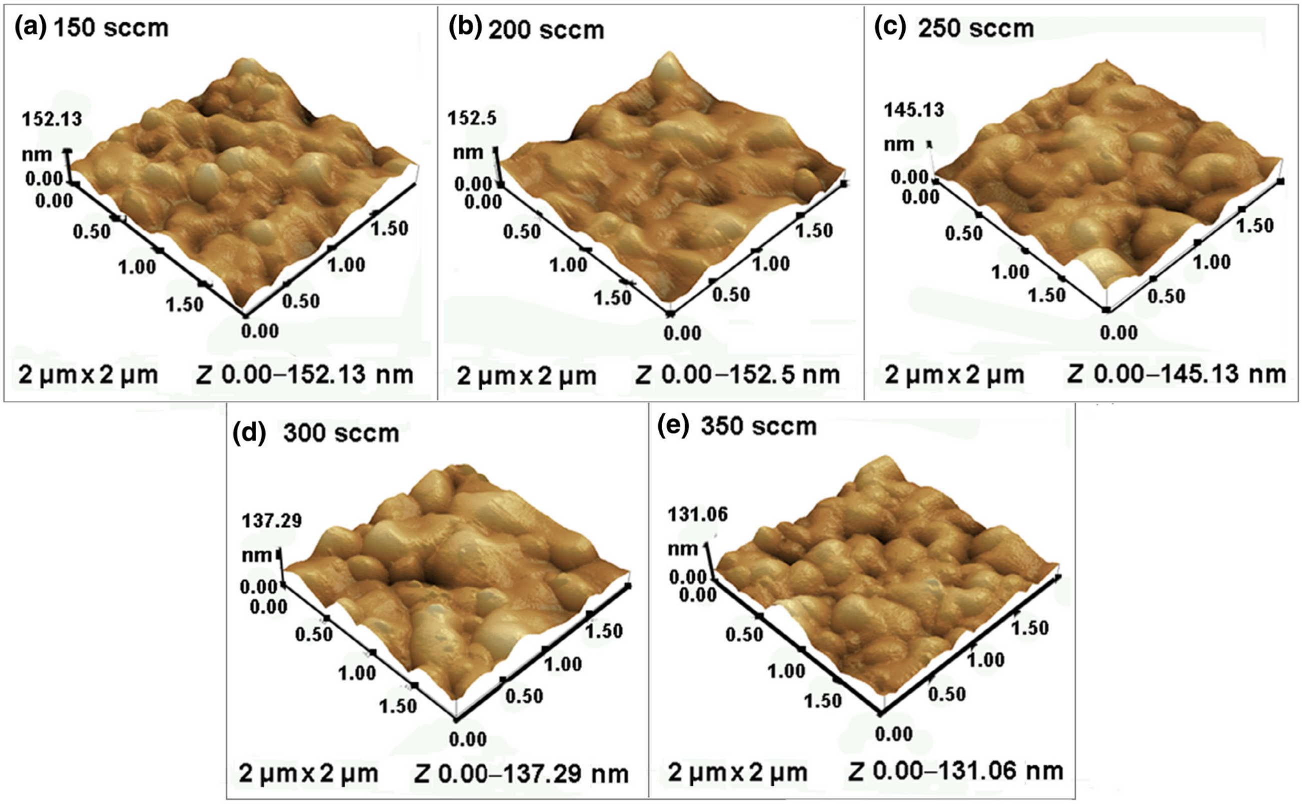

Fig. 4 AFM image of TiBCN films on Si(100) substrate by PVD at N_2 flow rates of 150–350 sccm

Fig. 5 Selected area electron diffraction patterns of **a** Ti interlayer and **b** TiBCN coatings

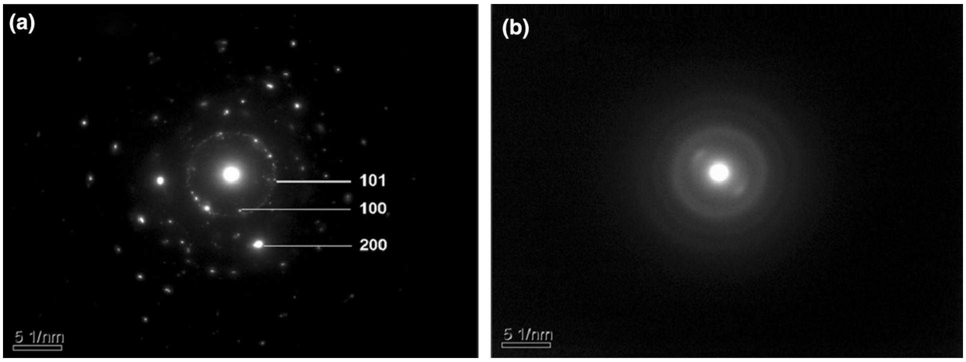

Ti hexagonal structure, which is consistent with the XRD results, showing the strongest Bragg reflection {101} and weak reflections of {100} and {200}. In the SAD of the TiBCN coating (Fig. 5b), a diffused halo was observed, indicating the amorphous properties of TiBCN films.

The high-resolution TEM images of TiBCN films are shown in Fig. 6. Clearly there are some nanocrystals embedded in the amorphous matrix, corresponding to TiB(211), $Ti_{0.68}N_{0.22}B_{0.1}$(102), TiB_2(101), BN (012) and TiN(101) and (200) in Fig. 6a–d, respectively. The size of the particles is 2–10 nm, and the distance between two nanoparticles is about 10 nm. Due to the limited content of nanocrystals embedded into a large fraction of the amorphous phase, it is difficult to find evidence by XRD, though it is clear in HRTEM.

XPS spectra of the TiBCN films at different N_2 flow rates are shown in Fig. 7. The XPS peaks were de-convoluted to provide further information about the films. Gaussian fitting was performed to evaluate the contribution of various factors in the spectra, and the fitted curves are shown in color lines. The Gaussian curves contributing to the fitting are represented by a dashed line. The B 1*s* spectrum of TiB_2 in Fig. 7a is ascribed to two peaks which correspond to TiB_2 (187.59 eV) [14] and B_2O_3 (192.6 eV), respectively. The B 1*s* of TiBCN-40 shows three peaks at 188.4, 189.7 and 191.6 eV, corresponding to

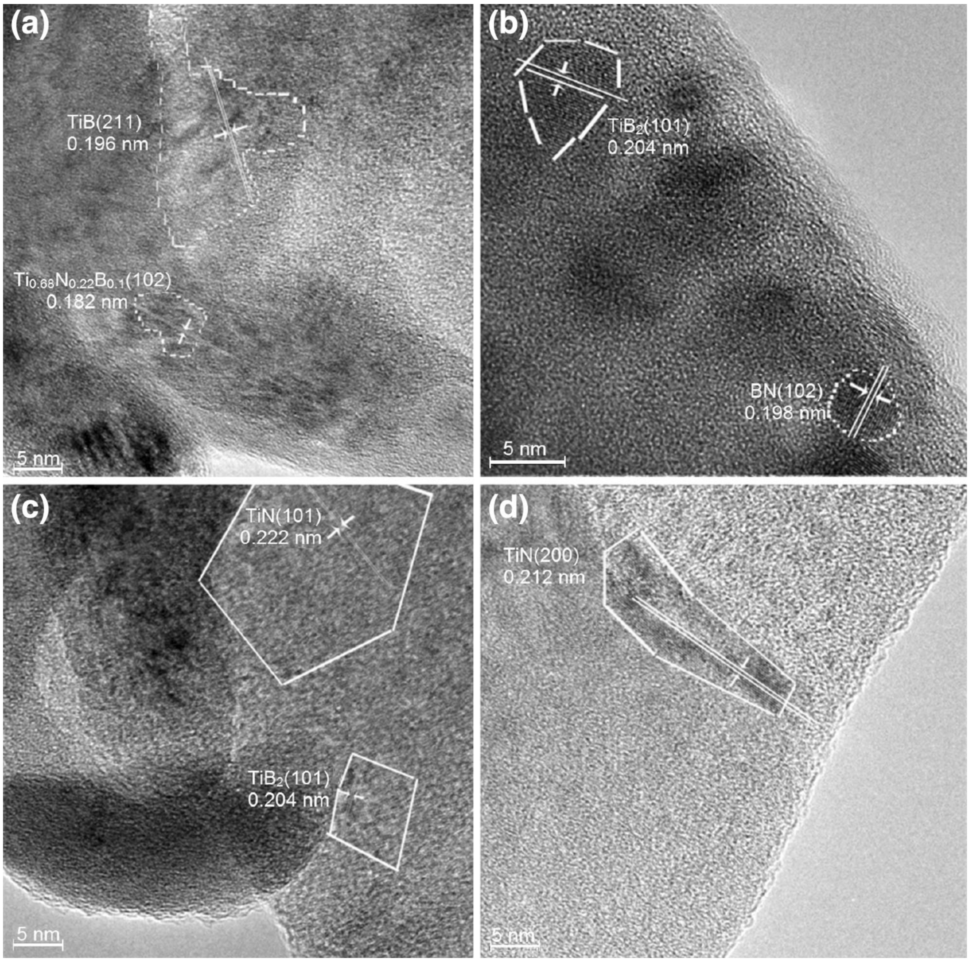

Fig. 6 High-resolution TEM images of TiBCN nanocomposite coatings deposited at N_2 flow rates of 250 sccm. **a**, **b**, **c** and **d** show different areas of TiBCN coatings and present different nanocrystal phases

Ti(B,C), BN and BNO, respectively. The peak at 188.4 eV indicates that the environment around the boron atom in the TiB_2 structure is modified with increasing C content [15]. BN is amorphous in nature, as proved by XRD. In the Ti 2*p* spectrum of TiB_2 (Fig. 7b), the peaks at around 454.3, 455.2, 457.6 and 458.7 eV are attributed to TiB_2 [14], TiO, Ti_2O_3 [16] and TiO_2 [17], respectively. In the Ti 2*p* spectrum of TiBCN-40, the peaks at 454.9, 455.8 and 458.9 eV are of TiC [5, 18], TiN [19] and TiO_2. After the Gaussian fitting, C 1*s* line is decomposed into two peaks which arise due to sp^2 C–C (284.5 eV) [15, 21] and sp^3 C–C (285.4 eV) [22] (Fig. 7c). In Fig. 7d, two peaks of N 1*s* spectrum of TiBCN-40 are ascribed to the amorphous N–C (399.3 eV) [6] and Ti–N (397.5 eV) [20]. The comparative study of B 1*s*, Ti 2*p*, C 1*s* and N 1*s* spectra for TiB_2 and TiBCN-40 films indicates that adding of C_2H_2 and N_2 influences the content of elements to a great extent, which leads to the sharp dropping of Ti and B content and increasing C and N contents. The films composition varied greatly, after adding N_2 and C_2H_2, the TiB_2 became Ti(B,C), TiN and TiC, forming amorphous phases, such as BN, CN_x, sp^2 C–C and sp^3 C–C.

Figure 8a shows the B 1*s* spectra at the N_2 flow rate of 40–350 sccm. The peak at 190.3 eV is BN [5, 23], and 189.2 eV is pure B [14]. It can be seen that the B–N peak increases with the N_2 flow rate, while the B content decreases with increasing N_2 flow rate. The peaks at 284.5 and 285.4 eV in Fig. 8b are related to sp^2 C–C and sp^3 C–C, respectively. Figure 8c shows the N 1*s* spectra of TiBCN at the N_2 rate flow of 40–350 sccm. At the low N_2 flow rates, the two peaks can be assigned to N–C (399.3 eV) and Ti–N (397.5 eV). At higher flow rates of N_2, BN (398.2 eV) [5, 17] appears and N–Ti shifts to 397.1 eV. The B–N and N–C peaks increase with the flow rate of N_2, while TiN (397.1 eV) shows different trends. Ti 2*p* spectra at the N_2 flow rate of 40–350 sccm are shown in Fig. 8d. The peak at 456.7 eV, corresponding to Ti(C, N) [5, 24], increases with the N_2 flow rate. The TiN position shifts to 455.6 eV [24]. The peak position at 458.5 eV is TiO_2 $2p_{3/2}$, due to oxidation of the surface of the TiBCN layer.

With increasing flow rate of N_2, the phases of TiN, Ti(C,N), amorphous carbon, amorphous BN and pure B changed differently. The content of sp^3 C–C (285.4 eV)

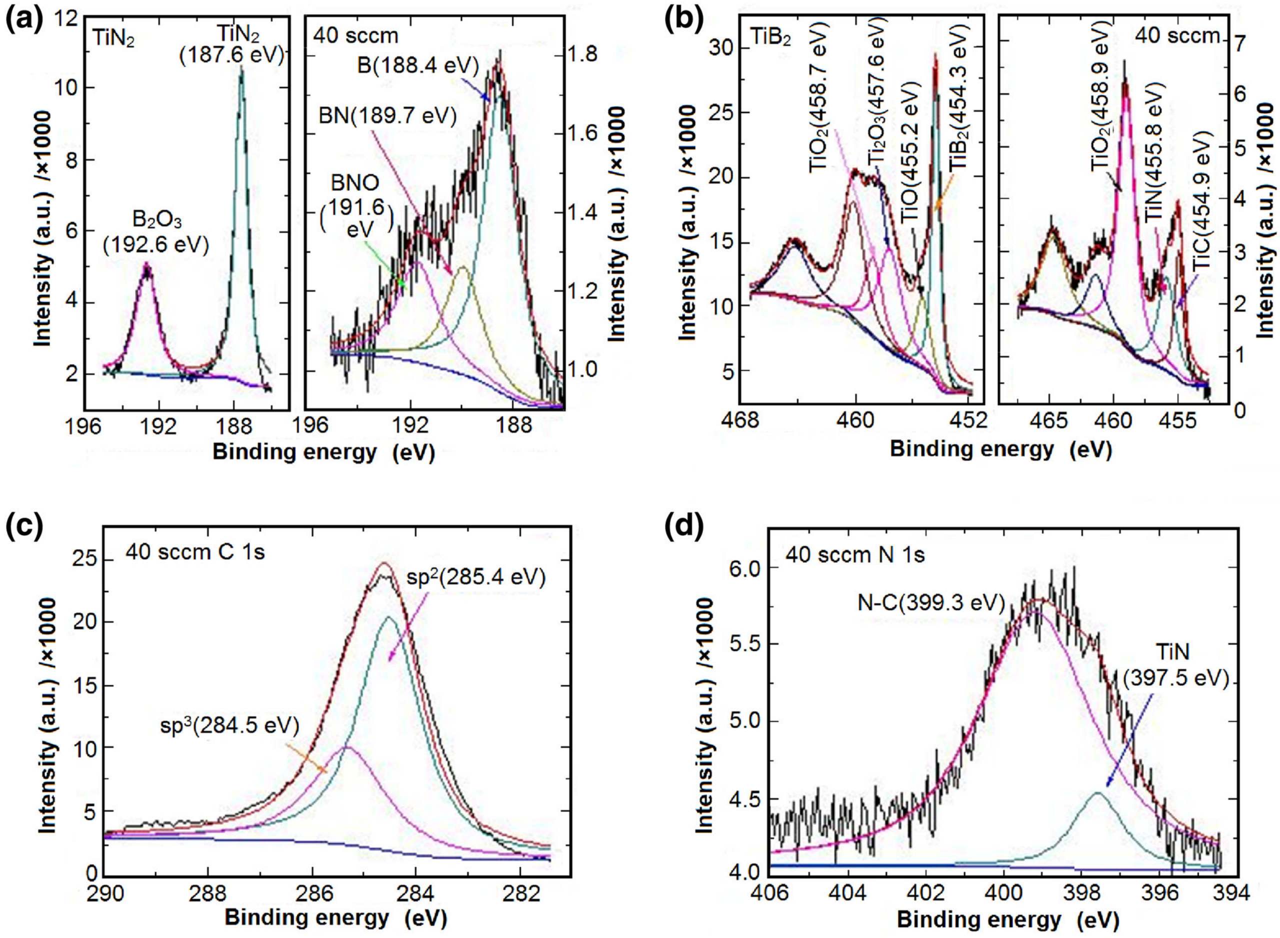

Fig. 7 XPS spectra of B 1*s* (**a**) and Ti 2*p* (**b**) from TiB_2 and TiBCN-40, and C 1*s* (**c**) and N 1*s* (**d**) from TiBCN-40

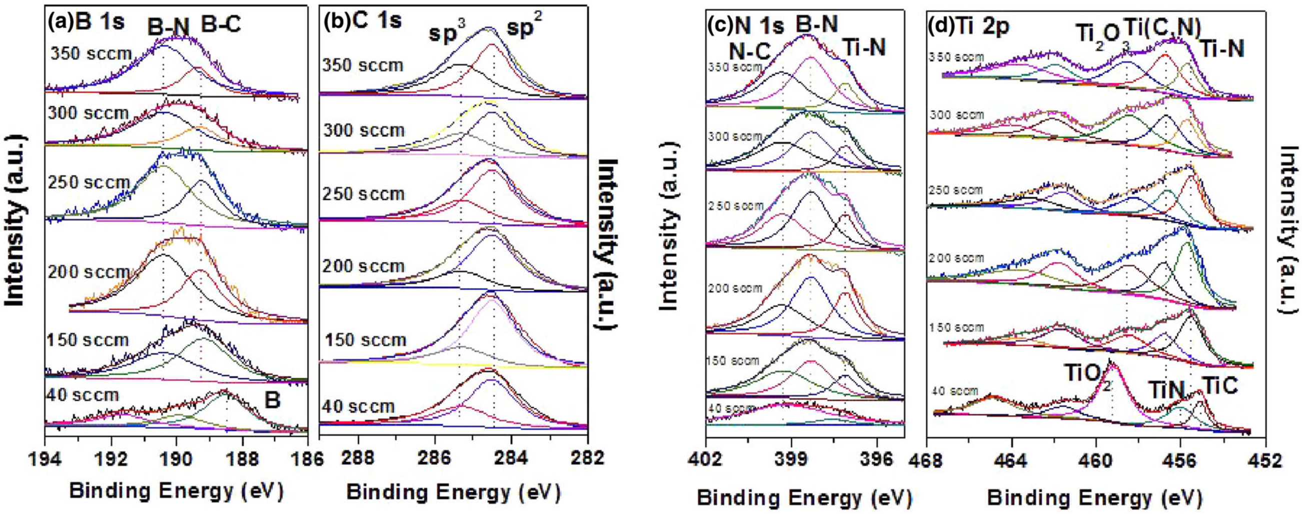

Fig. 8 XPS spectra of TiBCN prepared at N_2 flow rates of 40–350 sccm. **a** B 1*s*, **b** C 1*s*, **c** N 1*s*, **d** Ti 2*p*

and TiN (397.1 eV) are plotted in Fig. 9, as a function of the N_2 flow rate. The *sp*^{3} content decreased to a minimum at 150 sccm, where it began to increase, whereas the TiN content increased to a maximum at 200 sccm and then decreased, being the same changing trend as that of TiN (455.6 eV) in Ti 2*p* spectra.

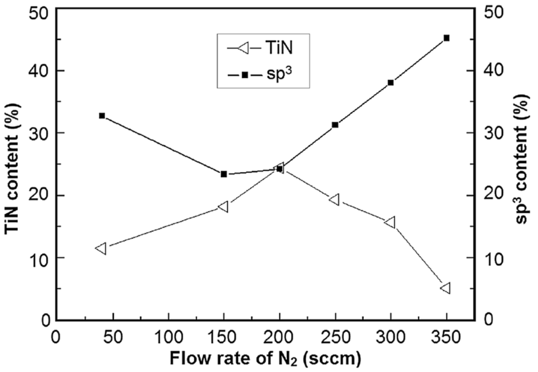

Fig. 9 Contents of TiN and sp^{3-} C–C evaluated from XPS measurement at the N_2 flow rates of 40–350 sccm

Amorphous phase BN, observed first at 150 sccm, increased with the N_2 flow rate, while pure boron, observed at 150 sccm, decreased with increasing N_2 flow rates.

It can be seen that the growth of TiBCN films is affected significantly by the gas flow rate. At 40 sccm, the Ti atoms mainly bond with B and C atoms, just a small fraction of them bond with N atoms. At 150 sccm, Ti atoms become to bond with N atoms, resulting in excess B being present in single-element phase and in less C–Ti bonds, which leads to free C atoms becoming hybridized. At maximum amount of TiN at 200 sccm, amorphous BN and CN_x are formed while pure B becomes less. With even more N_2 in the growing procedure, the large amount of C_2H_2 and N_2 gases in the chamber favors Ti atoms to bond with N atoms [4] and form TiN on the surfaces, but the collisions between C, N, B and Ti atoms never stop; thus, excess C and N atoms will collide with TiN crystallites on the surface and incorporate into TiN, resulting in Ti(C,N) at the expense of TiN.

There are two steps influencing sp^3 content at different N_2 fluxes: (1) at low fluxes of N_2, Ti atoms bond with B and C atoms, and sp^2 C–C bonding is disordered due to incorporation of Ti and B, hence the large sp^3 content, while at higher fluxes of N_2, Ti atoms become to bond with N atoms; then, sp^2 C–C is recovered and sp^3 C–C content decreases; (2) at fluxes over 200 sccm, there are less Ti atoms to bond with N atoms, excess N atoms will incorporate with sp^2 C–C, leading to increase in sp^3 C–C containment.

4 Conclusion

TiBCN films deposited by multi-cathodic arc ion plating were characterized by RBS, XPS, XRD, SEM and AFM measurements. It was found that the TiBCN films consisted of nanocrystals including TiN, TiB_2, TiB and $Ti_{0.68}N_{0.22}B_{0.1}$, with sizes less than 10 nm and amorphous matrix including BN, a-C, and CN_x. XRD showed main peaks from Ti interlayer and $TiN_{0.3}$ of the TiBCN films, with weak peaks from $TiN_{0.7}C_{0.3}$(200) and TiB(100). Cross-sectional SEM images showed the density of micro-particles on the surface decreasing with the N_2 flow rates. XPS showed bindings characteristic of B–N, Ti–N, Ti–O, B, sp^2 C–C, sp^3 C–C and N–C in TiBCN films. The TiN content increased first with the N_2 flow rates and then decreased, being favorable for the formation of Ti(C,N). The BN and CN_x contents increased at the expense of pure B content. The sp^3 content decreased to a minimum and then increased slowly, indicating the bonding of N atoms with Ti atoms and excess N atoms, tending to form N–C bonding.

References

1. H. Holzschuh, Chemical-vapor deposition of wear resistant hard films in the Ti–B–C–N system: properties and metal-cutting tests. Int. J. Refract. Met. H. **20**, 143–149 (2002). doi:10.1016/s0263-4368(02)00013-6
2. I. Dreiling, D. Stiens, T. Chassé, Raman spectroscopy investigations of $TiB_xC_yN_z$ films deposited by low pressure chemical vapor deposition. Surf. Coat. Technol. **205**, 1339–1344 (2010). doi:10.1016/j.surfcoat.2010.09.022
3. P.C. Tsai, W.J. Chen, J.H. Chen et al., Deposition and characterization of TiBCN films by cathodic arc plasma evaporation. Thin Solid Films **517**, 5044–5049 (2009). doi:10.1016/j.tsf.2009.03.029
4. S. Shimada, M. Takahashi, J. Tsujino et al., Deposition and wear resistance of Ti–B–N–C films on WC–Co cutting tools from alkoxide solutions by thermal plasma CVD. Surf. Coat. Technol. **201**, 7194–7200 (2007). doi:10.1016/j.surfcoat.2007.01.041
5. J. Lin, B. Mishra, J.J. Moore et al., Effect of asynchronous pulsing parameters on the structure and properties of CrAlN films deposited by pulsed closed field unbalanced magnetron sputtering (P-CFUBMS). Surf. Coat. Technol. **202**, 1418–1436 (2008). doi:10.1016/j.surfcoat.2007.06.068
6. F. Saugnac, F. Teyssandier, A. Marchand, Characterization of C–B–N solid solutions deposited from a gaseous phase between 900 and 1050°C. J. Am. Ceram. Soc. **75**, 161–169 (1992). doi:10.1111/j.1151-2916.1992.tb05459.x
7. M.D. Abad, J.C. Sánchez-López, M. Brizuela et al., Influence of carbon chemical bonding on the tribological behavior of sputtered nanocomposite TiBC/a-C films. Thin Solid Films **518**, 5546–5552 (2010). doi:10.1016/j.tsf.2010.04.038
8. L.L. Wang, R.Y. Wang, S.J. Yan et al., Structure and properties of Mo-containing diamond-like carbon films produced by ion source assisted cathodic arc ion-plating. Appl. Surf. Sci. **286**, 109–114 (2013). doi:10.1016/j.apsusc.2013.09.029
9. C. Rebholz, A. Leyland, P. Larour et al., The effect of boron additions on the tribological behaviour of TiN films produced by electron-beam evaporative PVD. Surf. Coat. Technol. **116–119**, 648–653 (1999). doi:10.1016/s0257-8972(99)00260-1
10. H. Elmkhah, F. Mahboubi, A. Abdollah-Zadeh et al., Size-dependency of corrosion behavior for TiN nanostructure films deposited by the PACVD method. Mater. Lett. **82**, 105–108 (2012). doi:10.1016/j.matlet.2012.04.154

11. D.E. Wolfe, J. Singh, Synthesis and characterization of TiBCN films deposited by ion beam assisted, co-evaporation electron beam-physical vapor deposition (EB-PVD). J. Mater. Sci. **37**, 3777–3787 (2002). doi:10.1016/s0257-8972(02)00666-7
12. F. Sanchette, C. Ducros, T. Schmitt et al., Nanostructured hard films deposited by cathodic arc deposition: From concepts to applications. Surf. Coat. Technol. **205**, 5444–5453 (2011). doi:10.1016/j.surfcoat.2011.06.015
13. P.Z. Shi, J. Wang, C.X. Tian et al., Structure, mechanical and tribological properties of CrN thick films deposited by circular combined tubular arc ion plating. Surf. Coat. Technol. **228**, S534–S537 (2012). doi:10.1016/j.surfcoat.2012.04.041
14. C. Pfohl, A. Bulak, K. Rie, Development of titanium diboride films deposited by PACVD. Surf. Coat. Technol. **131**, 141–146 (2000). doi:10.1016/s0257-8972(00)00752-0
15. R. Gilmore, M.A. Baker, P.N. Gibson et al., Preparation and characterisation of low-friction TiB_2-based films by incorporation of C or MoS_2. Surf. Coat. Technol. **105**, 45–50 (1998). doi:10.1016/s0257-8972(98)00445-9
16. Z.A. Umar, R.S. Rawat, K.S. Tan et al., Hard TiCx/SiC/a-C: H nanocomposite thin films using pulsed high energy density plasma focus device. Nucl. Instrum. Meth. B **301**, 53–61 (2013). doi:10.1016/j.nimb.2013.03.007
17. R. Ali, E. Alkhateeb, F. Kellner et al., Chemical vapor deposition of titanium based ceramic films on low carbon steel: Characterization and electrochemical evaluation. Surf. Coat. Technol. **205**, 5454–5463 (2011). doi:10.1016/j.surfcoat.2011.06.014
18. J. Lin, J.J. Moore, W.C. Moerbe et al., Structure and properties of selected (Cr–Al–N, TiC–C, Cr–B–N) nanostructured tribological films. Int. J. Refract. Met. Hard. Mater. **28**, 2–14 (2010). doi:10.1016/j.ijrmhm.2009.07.012
19. J. Lin, J.J. Moore, B. Mishra et al., The structure and mechanical and tribological properties of TiBCN nanocomposite films. Acta Mater. **58**, 1554–1564 (2010). doi:10.1016/j.actamat.2009.10.063
20. Y.H. Lu, Z.F. Zhou, P. Sit et al., X-Ray photoelectron spectroscopy characterization of reactively sputtered Ti–B–N thin films. Surf. Coat. Technol. **187**, 98–105 (2004). doi:10.1016/j.surfcoat.2003.11.024
21. B. Yang, Z.H. Huang, H.T. Gao et al., Droplet-free TiC nanocrystal-containing diamond-like carbon films deposited by combined cathodic arc MF magnetron sputtering. Surf. Coat. Technol. **201**, 6808–6811 (2007). doi:10.1016/j.surfcoat.2006.09.082
22. Y. Zheng, X.L. Liu, H.F. Zhang, Properties of Zr–ZrC–ZrC/DLC gradient films on TiNi alloy by the PIIID technique combined with PECVD. Surf. Coat. Technol. **202**, 3011–3016 (2008). doi:10.1016/j.surfcoat.2007.11.004
23. Y.H. Lu, Y.G. Shen, Z.F. Zhou et al., Phase configuration, nanostructure evolution, and mechanical properties of unbalanced magnetron-sputtered Ti–C_x–N_y thin films. J. Vac. Sci. Technol. A **25**, 1539–1546 (2007). doi:10.1116/1.2784719
24. Q. Wang, F. Zhou, Z. Zhou et al., Influence of carbon content on the microstructure and tribological properties of TiN(C) films in water lubrication. Surf. Coat. Technol. **206**, 3777–3787 (2012). doi:10.1016/j.surfcoat.2012.03.041